Pulsar timing constraints on narrow-band stochastic signals

K. A. Postnov[ab*], N. K. Porayko[ab†]

[a] *Sternberg Astronomical Institute*

Sternberg Astronomical Institute, Universitetsky pr., 13, Moscow 119991, Russia

[b] *Faculty of Physics, Moscow M.V. Lomonosov State University, Leninskie Gory, Moscow 119991, Russia*

Abstract

We consider the sensitivity of the pulsar timing array (PTA) technique to specific kind of narrow-band stochastic signals in nano-Hz frequency range. Specifically, we examine the narrow-band signal produced by oscillating gravitational scalar potentials in the Galaxy (Gravitational Potential Background), which arise if an ultralight massive scalar field is the galactic dark matter. We have performed a Bayesian analysis of publically available data on 12 pulsars obtained by the NANOGrav project. In the monochromatic approximation, the upper limit on the variable gravitational potential amplitude is $\Psi_c < 1.14 \times 10^{-15}$, corresponding to the dimensionless strain amplitude $h_c = 2\sqrt{3}\Psi_c < 4 \times 10^{-15}$ at frequency $f = 1.75 \times 10^{-8}$Hz. In the narrow-band approximation, the upper limit on the energy density of GPB is found to be $\Omega_{\rm GPB} < 1.27 \times 10^{-9}$ at $f = 6.2 \times 10^{-9}$Hz. These limits are an order of magnitude higher than the theoretically expected values, if the ultralight scalar field with a mass of $\sim 10^{-23}$ eV is assumed to be the galactic dark matter with a local density of ~ 0.3 GeV cm^{-3}.

1 Introduction

Direct detection of gravitational waves (GWs), predicted by general relativity (GR), stands among the principal challenges in experimental astrophysics during the last few decades. Measurements of the orbital decay of the binary pulsar J1915+1606 and similar systems [1] remain so far the strongest observational evidence for GW emission by space systems. Prompt development of GW detectors and projects, including ground-based and space interferometers, pulsar-timing and measurement of the anisotropy of cosmic microwave background, will likely result in the direct detection of GWs in the near future (see recent reviews [2, 3]).

A high stability of spin frequency of pulsars, especially old recycled millisecond pulsars, allows GW detection in pulsar timing measurements [4, 5]. A pulsar-timing GW detector is represented by two "free" masses: Earth and a pulsar. In the presence of a GW, electromagnetic signal from the pulsar, when traveling in perturbed spacetime, undergoes the frequency shift. As a result, the variations with particular form in times of arrival (TOA) of pulses from the given pulsar, which are usually measured in pulsar timing experiments, arise [6]. The main difficulty in detecting, for example, a monochromatic GW using this method is that variations in the pulsar timing residuals can be also caused by inaccurate measurements of the pulsar model parameters and the signal propagation in the interstellar space, therefore the timing residuals should be accurately cleaned from many possible contaminating effects.

The pulsar-timing procedure is sensitive to GWs in the frequency range which is limited by the Nyquist frequency (as determined by the duty cycle of the measurements, about two

*e-mail: pk@sai.msu.ru

†e-mail: porayko.nataliya@gmail.com

weeks) and by the entire time span of the observations (usually several years), i.e. $f_{\rm GW} \in [10^{-9}{\rm Hz}; 10^{-7}{\rm Hz}]$. As the GW detection procedure is determined by properties (amplitude, spectrum, etc.) of the sought signal, the searching strategies usually aim at detecting GWs from dominant sources in this frequency range, for example from supermassive black-hole binaries (SMBHBs) [7], which are presumably located in galactic centers, and from the stochastic gravitational wave background (GWB) produced by the whole population of extragalactic SMBHBs [8] or, likely, by several bright sources above a weak GWB [9, 10].

The idea of pulsar-timing Arrays (PTAs) was proposed in [11]. Besides the improvement in sensitivity to deterministic GW signals, the usage of data from several pulsars offers the possibility to search for stochastic GW background by cross-correlating timing residuals from different pulsars [12]. Several different PTA projects are currently running: EPTA [13], PPTA [14], NANOGrav [15], joined in the intrenational project IPTA [16] (see [17] for a review of the PTA techniques).

In addition to the "traditional" GW sources and stochastic backgrounds that can be probed in the PTA frequency range, there can be more exotic signals, including, for example, GWs from oscillating string loops [18], GW signals with memory [19, 20], GWs from massive gravitons [21, 22, 23, 24], etc.

Recently, Khmelnitsky and Rubakov [25] considered a model of an ultralight scalar field with bosons mass $m \simeq 10^{-23} - 10^{-24} eV$ as a warm dark matter candidate. Ultralight scalar fields as dark matter have been discussed in the literature: see e.g. Ref. [26, 27, 28, 29, 30] and references therein. In this model, due to unusually low boson mass, the dark matter density perturbations should be suppressed on subgalactic scales and would behave as the classical cold dark matter on scales larger than the Jeans wavelength $r_J = 150 kpc (10^{-23} eV/m)^{\frac{1}{2}})$. Moreover, all inhomogeneities are smoothed on scales shorter than the de Broglie wavelength $\lambda = 1/(mv) \simeq 600 pc (10^{-23} eV/m)(10^{-3} c/v)$, where v is the paricle velocity in the Galaxy. As the occupation number of dark matter particles in the galactic halo is huge, the collection of ultra-light particles can be described by a classical scalar field oscillating with frequency m. In turn, these oscillations would produce an oscillating pressure at frequency $\omega = 2m$ which is averaged to zero on time-scales larger than the period of oscillations. This makes the ultralight scalar field effectively non-interacting both with its own particles and particles of the Standard model. However, the pressure oscillations would result in variations in the scalar gravitational potentials, which can be probed by the PTA technique in a similar way as traditional GWs. Note that through a dilatonic coupling with the standard model particles, these oscillations could also be probed by atomic clock experiments [31].

The effect of the oscillating gravitational potentials on time arrival residulas from a pulsar is different from GWs: the response of each detector Earth-pulsar is independent of the source location on the sky, and the scalar field itself is not an individual source with given angular position. As the distances to pulsars are usually exceed de Broglie wave of the field (~ 600 pc for the fiducial mass of the field $m = 10^{-23}$ eV), the pulsar signal would propagate through regions with uncorrelated field phase, producing a stochastic narrow-band signal in the TOA residuals. To search for the imprint of the scalar field in pulsar timing data we have used data from NANOGrav Project, which are described in detail in Ref. [32].

2 Pulsar-timing response on the massive scalar field

A scalar field oscillating with frequency $\approx m$ can be represented as a collection of almost monochromatic ($\Delta\omega/\omega \sim v^2 \sim 10^{-6}$) plane waves, producing the oscillating pressure, and hence, through purely gravitational coupling, the variable scalar gravitational potentials $h_{00} = 2\Phi$ and $h_{ij} = -2\Psi\delta_{ij}$ (in the Newtonian conformal gauge) at frequency $\omega = 2\pi f = 2m$. In the weak field approximation two potentials converge to classical Newtonian potential and become equal to each other. As an electromagnetic signal from a pulsar travels through the time-dependent

spacetime, the irregularity in the strict periodicity of TOAs of pulses occurs. Physically, this effect is similar to the classical Sachs-Wolfe effect [33, 34].

The frequency shift of an electromagnetic wave propagating in the variable scalar potential background is [35]:

$$\frac{\nu(t'') - \nu(t')}{\nu(t')} = \Psi(\boldsymbol{x_{obs}}, t'') - \Psi(\boldsymbol{x_{em}}, t') - \int_{t'}^{t''} n_i \partial_i (\Phi + \Psi) dt, \tag{1}$$

where $\boldsymbol{x_{obs}}, t''$ and $\boldsymbol{x_{em}}, t'$ are the coordinate and time of the receiver and emitter, respectively. The value of the integral term in the above formula is suppressed by the small factor $k/\omega = v \sim 10^{-3}$ relative to the amplitude of potentials. Thus, only the variable part of the potential Ψ_c, which can be associated with the local dark matter density and the field mass as $\Psi_c \sim \rho_{\rm DM}/m^2$ [25], contributes to the pulsar timing signal.

The form of the resulting signal in TOA is:

$$R(t) = \frac{\Psi_c}{2\pi f} \left\{ (\sin(2\pi f t + 2\alpha(\mathbf{x}_e)) - \sin(2\pi f (t - D/c) + 2\alpha(\mathbf{x}_p)) \right\}, \tag{2}$$

where f is the frequency, D is the distance to the pulsar, c is the speed of light, $\alpha(\mathbf{x}_e)$ and $\alpha(\mathbf{x}_p)$ are the field phases on Earth and at the pulsar, respectively, and Ψ_c is the variable potential amplitude to be constrained from the PTA timing analysis.

The particular feature of this signal is that the signal amplitude does not depend on the angular distance between the source and the pulsar. Below, we will refer to the first and second terms in Eq. (2) as the "Earth-term" and "pulsar-term", respectively.

2.1 Monochromatic approximation

The expected signal is concentrated within a very narrow frequency band $\delta f/f \sim v^2 \sim 10^{-6}$, which is much smaller than the current PTA frequency resolution $\Delta f/f \sim 10^{-4}$, so we can neglect the signal broadening and consider the signal as monochromatic. In this approximation, the signal is given by Eq. (2).

However, the "pulsar-terms" add up at different phases due to low accuracy in the distance determination to pulsars. Usually, the "pulsar-term" is dropped and treated as part of the noise. Here we will analyze both cases (including and dropping the pulsar term) in Eq. (2). We will denote the effective phase angle due to the pulsar $\theta \equiv \alpha(\mathbf{x}_p) - \pi f D/c$, which is individual for each pulsar and is assumed to be uniformly distributed within the interval $[0, 2\pi]$.

2.2 Narrow-band approximation

In this approximation the signal is treated as a narrow-band stationary stochastic background with power contained within the frequency band δf around the central frequency f. The narrow-band background can be treated in the same way as stochastic GWB, however, some differences do arise due to different geometrical structures of GWs and a variable gravitational potential signal. We begin with comparing the case of the oscillating GPB with classical stochastic GWB [36, 22].

The properties of a stationary statistically homogeneous and isotropic GW field can be fully described by the metric power spectrum $P_h(k)$ per logarithmic interval of wave numbers $k = 2\pi f/c$:

$$\langle h_s(k^i) h^*_{s'}(k'^i) \rangle = \delta_{ss'} \delta^3(k^i - k'^i) \frac{P_h(k)}{16\pi k^3}, \tag{3}$$

where the angular brackets denote ensemble averaging over all possible realizations, the mode functions $h_s(k^i)$ correspond to plane monochromatic waves, and $s = 1, 2$ correspond to two linearly independent modes of polarization.

In the case of a narrow-band signal concentrated within some theoretically prescribed interval δk, it is essential to introduce the spectral amplitude P_0

$$P_h(k') = \begin{cases} P_0, k < k' < k + \delta k \\ 0, \text{in other cases.} \end{cases} \tag{4}$$

This allows us to relate h_c and P_0:

$$h_c^2 = \langle h^2 \rangle = P_0 \delta f / f \, . \tag{5}$$

From above equation we see that the energy parameter is $P_0 \delta f$.

It is also customary to relate the characteristic strain amplitude $h_c(k)$ to the energy density of a stochastic background per logarithmic frequency interval

$$\rho_{\rm GWB} = (16\pi G)^{-1} 4\pi^2 f^2 h_c^2, \tag{6}$$

or, in dimensionless units,

$$\Omega_{\rm GWB} = \frac{\rho_{\rm GWB}}{\rho_{cr}} = \frac{2\pi^2}{3H_0^2} f^2 h_c^2 = \frac{8\pi^2}{H_0^2} f^2 \Psi_c^2, \tag{7}$$

where the critical density is $\rho_{cr} = 3H_0^2/(8\pi G)$ and H_0 is the present-day Hubble constant.

In the PTA data analysis we also need the spectrum $S(f)$ of the TOA residuals produced by the sought stochastic signal, which can be obtained via transfer function of the residuals $\tilde{R}^2(k)$. For example, in the case of an isotropic GWB for the one-sided spectral density of the residuals, we obtain the well-known result

$$S_{\rm GWB}(f) = \frac{h_c^2}{12\pi^2 f^3}. \tag{8}$$

When deriving this formula, the averaging over the GW tensorial structure and polarization properties has been made. Repeating the derivation of the transfer function $\tilde{R}^2(k)$ as in Ref. [22] for the sought signal from oscillating scalar gravitational potential Ψ_c [Eq. (2)], we arrive at

$$S_{\rm GPB}(f) = \frac{\Psi_c^2}{\pi^2 f^3}, \tag{9}$$

which is 12 times as high as Eq. (8). This independently checks the relation between the equivalent GW characteristic strain h_c and the amplitude of the varying potential Ψ_c calculated in [25] [see their Eq. (3.9)]: $h_c = 2\sqrt{3}\Psi_c$.

As we are working in time domain, the knowledge of the covariance function C of the sought signal is needed. For a stochastic background, the variance covariance function C is related to the signal spectral density $S(f)$ via the Wiener-Khinchin theorem:

$$C(\tau) = \int_0^\infty S(f) \cos(\tau f) df \, . \tag{10}$$

Using the equation for the one-sided spectral density [Eq. (9)], we get:

$$C(\tau) = \int_0^\infty \frac{Q}{f^3} \cos(\tau f) df = Q\left(\frac{\tau \sin(f\tau)}{2f} - \frac{1}{2}\tau^2 \,\text{cosIntegral}(f\tau) - \frac{\cos(f\tau)}{2f^2}\right)\Bigg|_{f-\frac{\delta f}{2}}^{f+\frac{\delta f}{2}} . \tag{11}$$

This can be expanded in Maclaurin series:

$$C(\tau) = \frac{Q}{f^2}\left\{\cos(f\tau)\left(\frac{\delta f}{f}\right) - \frac{f^2\tau^2\cos(f\tau) - 12\cos(f\tau) - 6f\tau\sin(f\tau)}{24 f^3}\left(\frac{\delta f}{f}\right)^3 + O\left(\left(\frac{\delta f}{f}\right)^4\right)\right\} \tag{12}$$

Note that the coefficient before $(\delta f/f)^2$ is zero. Due to very narrow frequency range of the GPB signal, only the first term is retained. Thus, the covariance matrix C_{GPB} becomes:

$$C_{\rm GPB}(\tau_{ij}) = \zeta_{\alpha\beta}\frac{\Psi_c^2\delta f}{\pi^2 f^3}\cos(f\tau_{ij}), \tag{13}$$

where $\tau_{ij} = 2\pi|t_i - t_j|$, i and j are indexes of TOA, and f is the central frequency of the GPB under study. Here $\zeta_{\alpha\beta}$ is the correlation term between pulsars (α, β). As discussed above, GPB oscillations will induce a sinusoidal signal in the TOA of each pulsar with the correlation which takes the simple form (in contrast, for example, to the case of the GWB from merging SMBHBs):

$$\zeta_{\alpha\beta} = 1/2(1 + \delta_{\alpha\beta})\,. \tag{14}$$

Here the first and second terms arise due to the correlations between the pulsar term and the Earth term in Eq. (2), respectively.

3 Method of data analysis and data description

The algorithm of data treatment was implemented in the time domain in Ref. [37], which is commonly applied to unevenly sampled data to avoid the spectral leakage problem. Generally, pulsar-timing TOA $\mathbf{t}^{arr}$ contains deterministic and stochastic part:

$$\mathbf{t}^{arr} = \mathbf{t}^{det}(\boldsymbol{\beta}) + \boldsymbol{\delta}\mathbf{t}. \tag{15}$$

In this equation deterministic part is dependent on the pulsar model parameters $\boldsymbol{\beta}$.

In our analysis the stochastic part $\boldsymbol{\delta}\mathbf{t}$ is assumed to include three components. First component is white instrumental noise with the diagonal covariance matrix $C_{\rm WN}$. The red intrinsic noise can be characterized by the matrix $C_{\rm RN}$. The intrinsic pulsar red noise is a challenging problem in the pulsar-timing analysis because it strongly affects the PTA sensitivity to GW signals. The nature of this type of noise is not completely clear and can be related, for example, to irregular momentum exchange between the superfluid component and the neutron star crust, or to fluctuations of the electron density in the interstellar medium [38]. The red-noise spectrum is usually assumed to have a power-law form

$$S(f) = \frac{A^2}{12\pi^2}f_0^3\left(\frac{f}{f_0}\right)^{-\gamma}, \tag{16}$$

which is dependent on two parameters A_{RN} and γ_{RN} individual for each pulsar.

The last part corresponds to the oscillating GPB $C_{\rm GPB}$ (in the narrow-band approximation). Thus, the covariance matrix of the pulsar-timing data $\boldsymbol{\delta t}$ can be expressed as $C = C_{\rm WN} + C_{\rm RN} + C_{\rm GPB}$. The specific form of the white and red noise covariance matrices are discussed in [39].

In the time domain, we have implied the likelihood function technique to estimate the parameters of both the deterministic part and colored pulsar noise spectra [37]. After marginalization over unwanted pulsar model parameters $\boldsymbol{\beta}$, in the Bayesian approach we obtain the following expression for likelihood function, assuming the Gaussian distribution of $\boldsymbol{\delta t}$:

$$\begin{aligned} P(\boldsymbol{\delta}\mathbf{t}|\boldsymbol{\phi}) = &\frac{1}{\sqrt{(2\pi)^{(n-m)}\det(G^{\rm T}CG)}} \\ &\exp(-\frac{1}{2}\boldsymbol{\delta}\mathbf{t}^{\rm T}G(G^{\rm T}CG)^{-1}G^{\rm T}\boldsymbol{\delta}\mathbf{t}). \end{aligned} \tag{17}$$

Here n is the dimension of $\boldsymbol{\delta}\mathbf{t}$, m is a whole number of the unwanted parameters, $\boldsymbol{\phi}$ is the noise parameter vector, and G refers to the product of the so-called "design matrix" that can be obtained using the design matrix plugin of the TEMPO2 software [39, 40].

In the case of narrow-band stochastic process the spectral density (thus, the covariance matrix) of the sought gravitational potential is parameterized by Eq. (9) and depends on the dimensionless power of the stochastic background $\Omega_{\rm GPB}$ and central frequency f.

While searching for the deterministic signals (2), we have used the logarithmic likelihood ratio function which refers to the probability whether the signal is present or absent. In this case the function to be optimized depends on the amplitude Ψ_c and the Earth phase $\alpha(\mathbf{x}_e)$ of the scalar field when using the Earth term only, and on $N+2$ parameters: the amplitude Ψ_c, the Earth phase $\alpha(\mathbf{x}_e)$ and the phase $\theta_\beta = \alpha(\mathbf{x}_p^\beta) - \pi f D_\beta/c$, if both the Earth and pulsar terms are retained in the analysis.

The procedure of setting an upper limit on Ψ_c ($\Omega_{\rm GPB}$) as a function of the central frequency f is similar in both cases. We split the entire interesting frequency range into small bins per logarithmic scale [$\delta f/f \simeq 0.03 \ll 1/(5\,\mathrm{yrs})$]. In each bin we construct a long enough chain using Markov-chain Monte-Carlo method [41] in order to restore the posterior distribution of Ψ_c ($\Omega_{\rm GPB}$). The prior distribution for red-noise parameters A and γ was assumed to be multivariate normal, while for both amplitudes Ψ_c and $\Omega_{\rm GPB}$ the prior distributions were chosen to be uniform.

The obtained posterior distribution for Ψ_c and $\Omega_{\rm GPB}$, which turned out to be close to uniform one, was used to set upper limit on the amplitude. In other words, we estimate the Bayesian posterior distribution of the amplitude with MCMC method and assume that the amplitude of the probable signal with 95 % probability is limited by 0.95 quantile of the posterior distribution [42], taking into account uniform prior distributions. Results of this analysis are presented below in Sec. 4.

Methods described above were applied to real data from the NANOGrav Project. The observations were conducted during a 5-yr period from 2005 to 2010 using two radio telescopes, the Arecibo Observatory and NRAO Green Bank Telescope. The data are described in detail in Ref. [43] and are publicly available at [1]. To increase the signal-to-noise ratio in each observation, we have compressed the data by "daily averaging" TOAs [38]. Data from 12 pulsars have been analyzed. Four of them (J1713+0747, J2145-0750, B1855+09 and J1744-1134) show a weak red-noise component that have been estimated using the MCMC method. The post-fit residuals were obtained with the TEMPO2 software [40]. The additive and multiplicative factors (EFAC, EQUAD) were not been added to the "free parameter" template.

4 Results and Discussion

The nature of dark matter is unkown. One of the possible dark matter candidate in our Galaxy can be an ultralight scalar field (e.g. [25]). In this model, the dimensionless amplitude of the variable gravitational potential produced by the oscillating massive scalar field Ψ_c is related to the local galactic dark matter density $\rho_{\rm DM}$ and the field mass m as:

$$\Psi_c = \pi \frac{G\rho_{\rm DM}}{(\pi f)^2} \approx 10^{-16} \left(\frac{f}{10^{-8}\mathrm{Hz}}\right)^{-2} \approx 4.3\times 10^{-16} \left(\frac{m}{10^{-23}\mathrm{eV}}\right)^{-2} \left(\frac{\rho_{DM}}{0.3\mathrm{GeV\,cm^{-3}}}\right). \quad (18)$$

This field cannot be revealed using common telescopes aimed at the detection of electromagnetic signals, but can be probed with the pulsar-timing tool.

Working in the time domain we have applied the Bayesian approach developed in Ref. [37] to search for imprints of the oscillating gravitational potential in pulsar-timing data from the NANOGrav project. In our analysis we took into account the red noise for 4 pulsars in the array. The red-noise parameters were estimated using the MCMC method. In the data analysis, we examined three possible signal types: a monochromatic deterministic GPB with the Earth term only, a monochromatic GPB including both the Earth and pulsar terms, and a narrow-band

[1] http://www.cv.nrao.edu/~pdemores/nanograv_data/

stochastic GPB. In all cases we obtained upper limits on the signal amplitude Ψ_c (or $\Omega_{\rm GPB}$) as a function of frequency f. The best sensitivity is reached in the case of the monochromatic signal using both the Earth and pulsar terms.

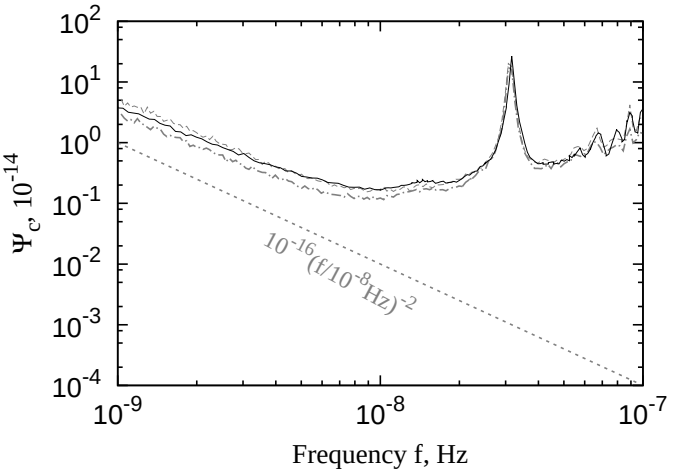

Figure 1: An upper limit on the amplitude of the variable gravitational potential Ψ_c due to the massive scalar field oscillations as a function of the central frequency f. Shown is the case of the narrow-band signal approximation (the black line), the monochromatic signal approximation with the Earth term only (the thin gray dashed line), and the monochromatic approximation using both the Earth and pulsar terms (the gray dashed-dot line); the lines are shown for the 95% confidence level. Data from eight pulsars from the NANOGrav Project with white-noise rms residuals were used. The dashed line shows the model amplitude (18).

Our upper limits are based on the Bayesian estimation of the signal amplitude. The Bayesian estimates can be biased because they do depend on the data realization. To obtain non-biased estimates (close to the true parameter values), it is necessary to make averaging over data realizations [44]

$$\hat{\theta} = \int_{X_n} \hat{\theta}_{\rm Bayes}(\mathbf{x}) W(\mathbf{x}) d\mathbf{x}, \tag{19}$$

where $W(\mathbf{x})$ is the "model evidence". In this case the estimates will be independent on the concrete realization of the data. We postpone the investigation of this effect for future work.

In the narrow-band approximation, the stringent limit on the field amplitude is $\Psi_c < 1.14 \times 10^{-15}$, which corresponds to the equivalent characteristic dimensionless strain $h_c = 2\sqrt{3}\Psi_c < 4 \times 10^{-15}$ at $f = 1.75 \times 10^{-8}$Hz (see Fig. 1). In this approximation the power spectral density of the GBP was assumed to have a delta-like form (4). Using a flat prior in the logarithmic scale, we numerically estimated the posterior distribution of the signal power in each frequency bin to set an upper limit on the GPB (in terms of $\Omega_{\rm GPB}$). In this case, the stringent upper limit is $\Omega_{\rm GPB} < 1.27 \times 10^{-9}$ at $f = 6.2 \times 10^{-9}$ Hz, which corresponds to $\Psi_c < 1.5 \times 10^{-15}$ (see Fig. 2). The sensitivity curves are similar in both monochromatic and narrow-band cases due to a particularly narrow frequency range of the stochastic signal [less than one frequency bin $\Delta f \sim 1/(5\,\mathrm{yr})$]. However, the narrow-band approach can be generally used to search for narrow-band stochastic signals of different origin.

The obtained limits are an order of magnitude higher than the theoretically expected values if the ultralight scalar field with a mass of $\sim 10^{-23}$ eV is assumed to be the galactic dark matter with a local density of ~ 0.3 GeV cm^{-3}.

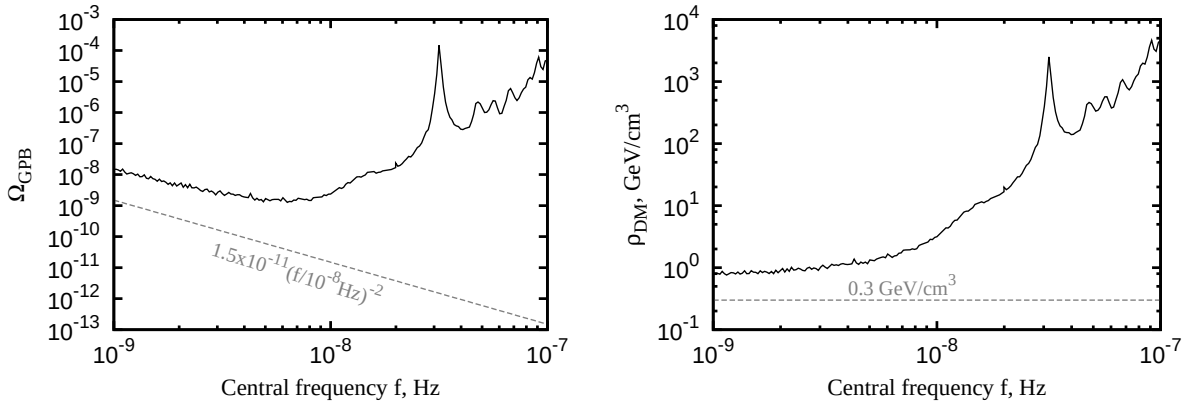

Figure 2: Left panel: An upper limit on the $\Omega_{\rm GPB}$ of the ultralight scalar field as a function of frequency f; the solid curve corresponds to the 95% confidence level. The dashed line shows the model value. Right panel: The same limit in terms of the local dark matter density $\rho_{\rm DM}$. The dashed line shows the local galactic dark matter density 0.3 GeV cm^{-3}. Data from 12 pulsars from the NANOGrav Project have been used.

Aknowledgements

The authors thank S. Babak, M. Pshirkov, V. Rubakov and A. Gusev for discussions for useful notes. The use of the publically available NANOGrav PTA data is acknowledged. The work is supported by the Russian Science Foundation grant 14-12-00203.

References

[1] C. M. Will. *ArXiv e-prints*, March 2014.

[2] Jonathan R. Gair, Michele Vallisneri, Shane L. Larson, and John G. Baker. *Living Reviews in Relativity*, 16(7), 2013.

[3] Nicols Yunes and Xavier Siemens. *Living Reviews in Relativity*, 16(9), 2013.

[4] M. V. Sazhin. *SvA*, 22:36–38, February 1978.

[5] S. Detweiler. *ApJ*, 234:1100–1104, December 1979.

[6] F. B. Estabrook and H. D. Wahlquist. *General Relativity and Gravitation*, 6:439–447, October 1975.

[7] F. A. Jenet, G. B. Hobbs, K. J. Lee, and R. N. Manchester. *ApJ*, 625:L123–L126, June 2005.

[8] A. Sesana, A. Vecchio, and C. N. Colacino. *MNRAS*, 390:192–209, October 2008.

[9] A. Petiteau, S. Babak, A. Sesana, and M. de Araújo. *Phys. Rev. D.*, 87(6):064036, March 2013.

[10] S. Babak and A. Sesana. *Phys. Rev. D.*, 85(4):044034, February 2012.

[11] R. S. Foster and D. C. Backer. *ApJ*, 361:300–308, September 1990.

[12] R. W. Hellings and G. S. Downs. *ApJ*, 265:L39–L42, February 1983.

[13] R. D. Ferdman, R. van Haasteren, C. G. Bassa, et al. *Classical and Quantum Gravity*, 27(8):084014, April 2010.

[14] R. N. Manchester, G. Hobbs, M. Bailes, et al. *Publ. Astron. Soc. Australia*, 30:17, January 2013.

[15] M. A. McLaughlin. *Classical and Quantum Gravity*, 30(22):224008, November 2013.

[16] R. N. Manchester and IPTA. *Classical and Quantum Gravity*, 30(22):224010, November 2013.

[17] A. N. Lommen and P. Demorest. *Classical and Quantum Gravity*, 30(22):224001, November 2013.

[18] T. Damour and A. Vilenkin. *Phys. Rev. D.*, 71(6):063510, March 2005.

[19] M. S. Pshirkov, D. Baskaran, and K. A. Postnov. *MNRAS*, 402:417–423, February 2010.

[20] R. van Haasteren and Y. Levin. *MNRAS*, 401:2372–2378, February 2010.

[21] S. L. Dubovsky, P. G. Tinyakov, and I. I. Tkachev. *Physical Review Letters*, 94(18):181102, May 2005.

[22] D. Baskaran, A. G. Polnarev, M. S. Pshirkov, and K. A. Postnov. *Phys. Rev. D.*, 78(4):044018, August 2008.

[23] M. Pshirkov, A. Tuntsov, and K. A. Postnov. *Physical Review Letters*, 101(26):261101, December 2008.

[24] K. Lee, F. A. Jenet, R. H. Price, N. Wex, and M. Kramer. *ApJ*, 722:1589–1597, October 2010.

[25] A. Khmelnitsky and V. Rubakov. *J. Cosmol. Astropart. Phys.*, 2:19, February 2014.

[26] M. I. Khlopov, B. A. Malomed, and I. B. Zeldovich. *MNRAS*, 215:575–589, August 1985.

[27] W. Hu, R. Barkana, and A. Gruzinov. *Physical Review Letters*, 85:1158–1161, August 2000.

[28] A. Arbey, J. Lesgourgues, and P. Salati. *Phys. Rev. D.*, 65(8):083514, April 2002.

[29] A. Suárez, V. Robles, and T. Matos. *ArXiv e-prints*, February 2013.

[30] Varun Sahni and Limin Wang. *Phys. Rev. D*, 62:103517, Oct 2000.

[31] A. Arvanitaki, J. Huang, and K. Van Tilburg. *ArXiv e-prints*, May 2014.

[32] P. B. Demorest, R. D. Ferdman, M. E. Gonzalez, et al. *ApJ*, 762:94, January 2013.

[33] R. K. Sachs and A. M. Wolfe. *ApJ*, 147:73, January 1967.

[34] R. K. Sachs, A. M. Wolfe, G. Ellis, J. Ehlers, and A. Krasiński. *General Relativity and Gravitation*, 39:1929–1961, November 2007.

[35] D. S. Gorbunov and V. A. Rubakov. *Introduction to the theory of the early universe*. World Scientific Pub. Co., Singapore; Hackensack, N.J., 2011.

[36] L. P. Grishchuk, V. M. Lipunov, K. A. Postnov, M. E. Prokhorov, and B. S. Sathyaprakash. *Physics Uspekhi*, 44:1, January 2001.

[37] R. van Haasteren and Y. Levin. *MNRAS*, 428:1147–1159, January 2013.

[38] A. N. Lommen and P. Demorest. *Classical and Quantum Gravity*, 30(22):224001, November 2013.

[39] R. van Haasteren, Y. Levin, P. McDonald, and T. Lu. *MNRAS*, 395:1005–1014, May 2009.

[40] G. B. Hobbs, R. T. Edwards, and R. N. Manchester. *MNRAS*, 369:655–672, June 2006.

[41] M. E. J. Newman and G. T. Barkema. *Monte Carlo methods in statistical physics*. 1999.

[42] R. van Haasteren, Y. Levin, G. H. Janssen, et al. *MNRAS*, 414:3117–3128, July 2011.

[43] D. Perrodin, F. Jenet, A. Lommen, et al. *ArXiv e-prints*, November 2013.

[44] B. R. Levin. *Theoretical fundamentals of statistical radiotechnics*. 1989.